01 Jan 1993

Detection of Skin Tumor Boundaries in Color Images

Fikret Erçal
Missouri University of Science and Technology, ercal@mst.edu

M. Moganti

William V. Stoecker
Missouri University of Science and Technology, wvs@mst.edu

Randy Hays Moss
Missouri University of Science and Technology, rhm@mst.edu

Detection of Skin Tumor Boundaries in Color Images

F. Ercal, M. Moganti, W. V. Stoecker, and R. H. Moss

Abstract— **Boundary detection has been recognized as one of the difficult problems in image processing and pattern analysis, in particular in medical imaging applications. There is no unified approach to this problem, which has been found to be application-dependent. In this paper, we present a simple and yet effective method to find the borders of tumors as an initial step towards the diagnosis of skin tumors from their color images. The method makes use of an adaptive color metric from the red, green, and blue (RGB) planes that contain information to discriminate the tumor from the background.**

Using this suitable coordinate transformation, the image is segmented. The tumor portion is then extracted from the segmented image and borders are drawn. Experimental results that verify the effectiveness of this approach are given.

I. Introduction

Boundary detection of objects is a fundamental problem in computer vision: boundaries represent a major fraction of the information content in an image. In this paper, we are particularly interested in finding the tumor borders in the context of automated diagnosis of skin tumors from their color images. The problem is complex because of other information corrupting the clarity of the image. We collectively refer to this other information, some of which may well be extraneous features, as noise. It is difficult to distinguish the correct borders of the objects of interest from the borders outlined due to this noise. The identification of object and surface boundaries comes naturally to a human observer, but accurate automatic image segmentation has proved to be difficult and complex. Detecting the tumor border is the first and the most important low-level processing to be done on the image, for without finding borders successfully, much of the information used in the diagnosis (higher level processing) cannot be accurate. In general, achieving an adequate segmentation result depends mainly on devising techniques to detect uniformity among the feature values of the picture points and then isolating the areas of the picture exhibiting these uniformities. Techniques such as edge detection, region growing, histogram thresholding, and clustering have been used. Among these, the last two methods have been extensively used for segmenting color images [1]–[3].

The actual outline of the boundary provides important information directly concerning almost all of the features that were identified to be useful in diagnosis, such as border irregularity and asymmetry [4], [5]. Researchers have sought to detect tumor boundaries accurately to allow skin cancer detection [5]–[7]. In spite of all efforts, none of the proposed methods have been reported to be sufficiently reliable on large numbers of tumor images. An algorithm called *radial search*, described and implemented in [5], makes use of luminance as the primitive border determinant. This algorithm starts in the center of the object, and by searching outward along radial lines attempts to find points that are likely border points. It operates on gray-scale images, looking for significant jumps in luminance that are sustained, and relaxing the jump and sustained distance thresholds repeatedly to find the optimal border. The problem with radial search is that it finds false border points if the tumor-to-background transition is not reasonably sharp. It also assumes radial connectedness—that no radius intersects the border twice—which may be violated by some tumor images. In all, the radial search method is limited to accurate detection in fewer than 2/3 of tumor borders, obviously not satisfactory for the system to be useful. Instead of detecting individual border points, the new method presented here detects connected tumor segments from which border points are picked. This eliminates most of the spurious border points due to noise. This technique yields to a simple and yet effective method to find the borders. It makes use of an adaptive color metric obtained from R-G-B planes depending on which of the planes contain much of the information. A linear transformation from R-G-B space to $X(R, G, B)$ is performed at the preprocessing stage. After preprocessing, the image is segmented using both the tumor and the background information.

Manuscript received July 7, 1992; revised January 12, 1993.

F. Ercal, M. Moganti, and W. V. Stoecker are with the Department of Computer Science, University of Missouri–Rolla, Rolla, MO 65401.

This work was supported in part by the National Science Foundation under SBIR Phase II award number ISI-8521284 and the Intelligent Systems Center of the University of Missouri-Rolla.

IEEE Log Number 9210302.

II. Preprocessing and Measurements to Identify Border Determinants

In many practical applications such as this, the input image is often contaminated with a moderate to high level of noise induced primarily by the surrounding environment of the object sought. For example, Fig. 1(a) is a tumor image that has hair, flash reflections (bright portion in the tumor), scale, and eyelid as noise in the image. In addition to unnecessary objects of interest, all the images obtained are not of the same quality (due to differences in lighting, type of film used, etc.). In the case of noisy and low-quality images, the intensity distributions of the object and the background in a histogram become less identifiable, and the histogram obtained directly from the R-B-G data does not exhibit appreciable bimodality. Also, tumor portions that are of low contrast to the background form bad candidates to identify the borders. An iterative *median filter* [8] was applied to reduce the effect of the noise and to improve the visibility of the tumor borders clearly. A 3×3 window was used for median filtering, and 2 to 3 iterations were found to be very effective in generating filtered images suitable for segmentation. Furthermore, using histogramming, and an approximate color segmentation strategy, we could identify two small windows of size 20×20, one inside and one outside the tumor area. These windows were used later in obtaining color variances and a proper threshold for tumor and background colors.

The preprocessing step was followed by a color transformation to improve the bimodality of the image histogram. We experimented with various transformation functions to find the best set of characteristic determinants that would distinguish tumor colors from the background. In a previous study, Umbaugh compared a number of transformations, R, G, B, Y, Q, I (intensity), S (saturation), H (hue), and (L, a^*, b^*) (spherical transformations) to identify colors of skin tumors [3]. It was found that spherical transformations and chromaticity transformations provided the highest diagnostic accuracy when color data was provided to an automatic induction system. Ohta *et al.* [2] showed that a set of color features $I_1 = (R + G + B)/3$, $I_2 = (R - B)$, and $I_3 = (2G - R - B)/2$ are effective in segmenting various kinds of color pictures and compared their results with those obtained from the Karhunen-Loeve (KL) transformations. They concluded that the transformation coefficients for I_1, I_2, and I_3 are very close to those of KL. Our investigation into all the above color transformations has also shown that I_1 and I_2 are effective in discriminating the tumor from the background. The ineffectiveness of the standard color transforms show the domain dependency of

these transformations in an application. Dhawan [6] also used I_1, I_2, and I_3 for extracting intensity and texture-based features from the tumor images for segmentation. In our application, we found that the color transformation $X = w_r R + w_g G + w_b B$ is a good candidate for effective segmentation provided that the weights, w_r, w_g, and w_b are estimated as outlined below. In feature selection in pattern recognition theory, a feature is said to have large discriminant power if its variance is large. Thus we tried to first identify which of the three planes have large discriminating power to separate out tumor pixels from the background ones. More specifically, let S be the region to be segmented, and Ψ be the vector $\{v_r, v_g, v_b\}$ of the distributions of R, G, and B in S which is defined by

$$v_r = \sum_{i,j} (r_T(i,j) - r_{NT}(i,j))^2$$

$$v_g = \sum_{i,j} (g_T(i,j) - g_{NT}(i,j))^2$$

$$v_b = \sum_{i,j} (b_T(i,j) - b_{NT}(i,j))^2$$

where T and NT are small-size windows extracted from the tumor and the background skin respectively. We experimentally found that, if the windows are enclosed entirely within the tumor and the background skin respectively, a window size of (20×20) was large enough to compute the variances that turn out to be very close to those obtained by using the entire scene. The components of Ψ reflect to what extent each of the color planes help in isolating the tumor region from the background. The larger a component is, the more discriminative power it has. w_r, w_g, and w_b are obtained as the normalized components of the vector $\{v_r, v_g, v_b\}$:

$$w_r = \frac{v_r}{v_r + v_g + v_b}$$

$$w_g = \frac{v_g}{v_r + v_g + v_b}$$

$$w_b = \frac{v_b}{v_r + v_g + v_b}$$

The percent deviation Δ_i ($i = 1$ to 3) of these weights from that of the weights (e_1, e_2, e_3) belonging to the first component of the Karhunen-Loeve transform (obtained from the eigenvector corresponding to the largest eigenvalue containing the maximum variance) and their borders, over 15 images are given in Table I and Table II respectively. As shown in Table I, none of the components differ more than 25% while 82% of the components differ by less than 9%. Table II shows the rating of border quality by a dermatologist. This experiment shows that these three features nearly match the Karhunen-Loeve transformations and can be used successfully, thus reducing the cost of computation required for KL transform computations significantly.

TABLE I
PERCENT DEVIATION OF KL-TRANSFORM FROM X-TRANSFORM

Image No.	$\Delta_1 = \frac{(w_r - e_1)}{w_r}$	$\Delta_2 = \frac{(w_g - e_2)}{w_g}$	$\Delta_3 = \frac{(w_b - e_3)}{w_b}$
40	15.8	2.7	4.5
100	4.5	2.7	5.2
102	5.5	3.2	13.3
109	0.0	0.0	5.2
207	10.0	2.5	2.5
331	4.3	23.8	21.2
351	5.8	7.0	10.0
361	2.0	5.9	0.0
365	4.0	6.25	0.0
385	3.8	3.03	6.6
424	2.2	0.0	5.0
425	2.0	0.0	5.0
490	8.6	17.4	25.0
2016	3.5	2.6	2.9
2077	6.9	0.0	7.7

TABLE II
RESULTS OF KL-TRANSFORM AND X-TRANSFORM BORDERS

Program Type	Excellent	Good	Fair–Poor
KL-Transform Border	8	3	4
X-Transform Border	10	2	3

III. SEGMENTATION AND BOUNDARY TRACING

The object of interest (the tumor area) has distinctive pixel values in the transformed plane X—i.e., the tumor pixels have lower values than the background and can be easily extracted using thresholding. Thresholding is a widely used tool in image segmentation for identifying the different homogeneous components of the image. If an image has multiple objects of interest, the proper choice of threshold may vary from place to place in an image; it may be preferable to threshold an image in an adaptive manner. In this application, threshold selection has become simple because of only one object of interest. In addition to this fact, knowledge of the tumor and of the background portions made this threshold calculation easy; a simple threshold selection $\Gamma = (\frac{\mu_T + \mu_{NT}}{2})$ strategy worked consistently well, where μ_T and μ_{NT} are the means of the known tumor and background portions of the transformed image X. To measure the sensitivity of the system to the particular selection of Γ, we compared the percent errors occurred when using five different thresholds, equally spaced between μ_T and μ_{NT}: μ_T, $\frac{\mu_T + \Gamma}{2}$, Γ, $\frac{\mu_{NT} + \Gamma}{2}$, and μ_{NT} on segmenting 8 different tumor images. For each image, a region D, representing the dermatologist-determined tumor region, is compared to the region A, the automatically determined tumor region. The error measure $E = \frac{(A \cup D) - (A \cap D)}{D}$ is used, where $(A \cup D) - (A \cap D)$ represents the nonoverlapping area of the two binary images. Though $\Gamma = (\frac{\mu_T + \mu_{NT}}{2})$ is not an optimal threshold, it is found to generate the minimum percent errors (in 5 cases) or next to minimum (in 3 cases). In all cases, the increase in percent errors is significant when moving from the best threshold level to one of its neighbors.

The segmented image contains the true tumor cluster along with some background areas falsely identified as tumor clusters due to noise (refer to Fig. 1(b)). These non-tumor clusters are present due to the fact that these portions in the original image have tumor pixel characteristics. Also, because portions of the tumor in the original image have characteristics similar to the background, after segmentation, the tumor cluster contained holes. For example, Fig. 1(b) shows the tumor portion with one visible hole in it. Hence, finding the boundary points is done in two phases. First, the tumor segment is extracted from the image using a recursive region growing algorithm that starts with a tumor point as a seed point and recursively searches for tumor points in its neighborhood. After all the tumor points are exhausted, the algorithm stops, thus masking all the other unnecessary information around it. Fig. 1(c) is the segmented image with only the tumor portion where unnecessary information is masked out. Due to holes inside the tumor portion, the search for boundary points is not trivial. A contour-following algorithm as described in [9] is used to determine border points in their right order. This algorithm assumes four-connectedness which is appropriate for our application. Correct ordering of the boundary points is required for the spline operation which follows this step. We need to apply some sort of a spline for smoothing the resulting border for the reasons outlined below.

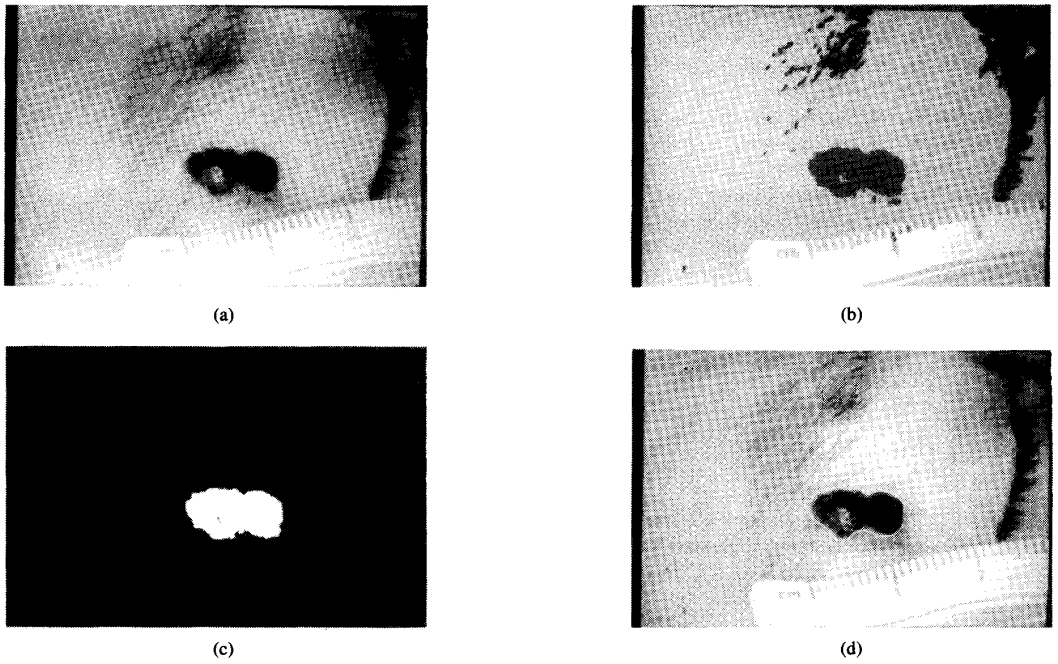

Fig. 1. Steps in automatic border detection (a) The original image (from New York University collection). (b) Segmented image with noise. (c) Segmented image without noise. (d) Splined border.

Pigmented lesions are almost always smoother than the automatically found border. Jaggedness in pigmented lesions occurs with coves and peninsulas of size greater than 1 mm and generally greater than 2 mm due to the scale of the pigmentation phenomenon in human skin, with a dermal papilla about 1 mm (coarse-grain irregularity). Automatically found borders often have small irregularities less than this, often a pixel or several pixels wide, representing a small fraction of a mm (fine-grain irregularity). These small irregularities represent errors in finding the actual shape of the perimeter as observed by a dermatologist. Smooth borders are obtained by picking up equally spaced points (control points) from the above generated points and connecting them by a cubic spline. A pathophysiological border descriptor *border irregularity*, I, associated with skin malignancy is one of the features used in the diagnosis. I is given as $I = (P^2/4\pi A)$ in [10], where P and A are the perimeter and area, respectively of the closed boundary along the tumor. The perimeter P is calculated by counting the number of pixels along the smooth border. P may turn out to be too high if the border contains fine-grain irregularities (due to the digitization process). On the other hand, selecting the control points sparsely for the cubic-spline would result in a highly smooth border which may hide the coarse-grain irregularities (notches, coves, peninsulas, etc.) that are actually present in the tumor. By experimentation, we found that control points that are 10 points apart resulted in an acceptable smoothing operation that preserved all the crucial elements at the border for the computation of the *irregularity index*, I, while removing the extra jaggedness originating from the digitization process. Fig. 1(d) shows the splined border outlined for Fig. 1(a).

IV. Experimental Results

We tested our border finding technique on 61[1] clinical dermatology images which were obtained by the digitization of 35mm color photographic slides. Images were put into different classes with respect to their tumor types, and the results are summarized in Table III, each row representing the border results obtained for images belonging to a specific tumor type. A dermatologist rated the borders determined by the algorithm as "excellent," "good," "fair," and "poor" depending on how close the border was to the one he perceived. Since the color change at the boundary of the tumor and the background is gradual, it is difficult to determine the exact borders with a human eye. Therefore, it is inevitable that the evaluation will be subjective. We used a dermatologist's expert opinion in order to minimize the error in the evaluation. A conservative approach was taken in the ratings; i.e., even a small deviation from the real border was considered to be a "poor" result. If we consider only those rated as "excellent" and "good" to qualify for success, then the overall percentage of success in detecting the borders is above 82%. This is a significant improvement over the 66% success rate of the previous *radial search* method [5]. Considering each class on its own, the lowest success rate is obtained for "melanoma" images at 77% and the highest success rate is achieved for "intradermal nevus" at 100%. These results show that our approach finds the tumor borders relatively independent from the tumor class at a reasonably high success rate. We also note that depending on how critical the application is, most of the results listed under the "fair" column may well be considered as successes. In this case, success rate would go up to 90% which is a significantly high ratio considering the fact that most of the images contain extraneous features such as hair, rulers, etc.

[1]The 61 slides were obtained from Dr. Stoecker's clinical collection and from New York University.

V. Conclusion

In conclusion, this paper presents a simple yet effective border-finding algorithm targeted to color images of skin tumors. The technique is based on a segmentation algorithm that uses an adaptive transformation function followed by thresholding. Over 80% of the borders found by the algorithm were in close agreement with those

TABLE III
EVALUATION BY A DERMATOLOGIST ON BOUNDARIES DETECTED

Tumor Type	Border Evaluation			
	Excellent	Good	Fair	Poor
Intradermal Nevus	3	3		
Melanoma	14	13	3	5
Seborrheic Keratoses	3	3	1	1
Dysplastic Nevi	7	4		1
Totals	27	23	4	7

identified by a dermatologist. This is a significant improvement compared to the earlier techniques proposed in the same domain [5], [7]. Our experience in this study also demonstrated that the strategies and the measurements used are application-dependent. Although good results were obtained for certain classes of tumors, the technique is not universal, as some classes of tumors have entirely different border determinants. Hence, our future work will concentrate on devising strategies to cover the other classes and on integrating these methods. Furthermore, we plan to extend our techniques to do color segmentation inside the tumor area itself to aid the diagnostic process in other ways.

ACKNOWLEDGMENT

The authors gratefully acknowledge Kathy Whyte for providing technical assistance, and William Slue of New York University for supplying some of the tumor images used in this study. Also the authors would like to acknowledge the reviewers for their valuable remarks and suggestions.

REFERENCES

[1] M. Celenk, "A Color Clustering Technique for Image Segmentation," *Computer Vision, Graphics and Image Processing*, vol. 52, pp. 145–170, 1990.

[2] Y. I. Ohta, T. Kanade, and T. Sakai, "Color Information for Region Segmentation," *Computer Graphics and Image Processing*, vol. 13, pp. 222–241, 1980.

[3] S. E. Umbaugh, "Computer vision in medicine: Color metrics and image segmentation methods for skin cancer diagnosis," Ph.D. dissertation, Dept. of Electrical Engineering, University of Missouri-Rolla, MO, 1990.

[4] F. Ercal, A. Chawla, W. V. Stoecker, and R. H. Moss, "Diagnosing Malignant Melonoma Using a Neural Network," *Intelligent Engineering Systems Through Artificial Neural Networks*, vol. 2, ASME Press, pp. 553–558, 1992.

[5] J. E. Golston, R. H. Moss, and W. V. Stoecker, "Boundary Detection in Skin Tumor Images: An Overall Approach and A Radial Search Algorithm," *Pattern Recognition*, vol. 23, no. 11, pp. 1235–1247, 1990.

[6] P. A. Dhawan and A. Sicsu, "Segmentation of images of skin lesions using color and texture information of surface pigmentation," *Computerized Medical Imaging and Graphics*, vol. 16, pp. 163–177, May 1992.

[7] S. E. Umbaugh, R. H. Moss, and W. V. Stoecker, "An automatic color segmentation algorithm with application to identification of skin tumor borders," *Computerized Medical Imaging and Graphics*, vol. 16, pp. 227–235, May 1992.

[8] A. Rosenfeld and A. C. Kak, *Digital Picture Processing*, 2nd ed., vol. I. Orlando, FL: Academic Press, 1982, pp. 261–264.

[9] Richard O. Duda and Peter E. Hart, *Pattern Classification and Scene Analysis* New York: Wiley, 1973, pp. 290–292.

[10] J. E. Golston, W. V. Stoecker, R. H. Moss, and I. P. S. Dhillon, "Automatic detection of irregular borders in melanoma and other skin tumors," *Computerized Medical Imaging and Graphics*, vol. 16, pp. 199–203, May 1992.

Comments on "A Note on Smith's Reconstruction Algorithm for Cone Beam Tomography"

Bruce D. Smith

***Abstract*—The counterexample developed in "A Note on Smith's Reconstruction Algorithm for Cone Beam Tomography" leads one to conclude that an equation in "Image Reconstruction from Cone-Beam Projections: Necessary and Sufficient Conditions and Reconstruction Methods" (*IEEE Trans. Med. Imaging*, vol. MI-4, Mar. 1985) is wrong. The objective of this correspondence is to discuss what effect such an error would have on the results given in this paper.**

I. INTRODUCTION

In [1] a counterexample is given that provides a contradiction between equations (5.6) and (2.5) given in [2]. Since (2.5) is presumably correct, this would lead one to conclude that (5.6) is wrong. The objective of this note is to discuss what effect such an error would have on the results given in [2].

II. DISCUSSION

A key theoretical result given in [2] is statement 5. In practical terms this statement implies that if on every plane that intersects the object there is a source point, then one can, in theory, produce an "exact" reconstruction. Furthermore, if there isn't a source point on every plane, then one has to do some extrapolation either explicitly using a method like Projections Onto Convex Sets (POCS) or implicitly using a method like the Expectation Maximization (EM) method. The need for extrapolation is further explained in [3].

A critical step in the development of statement 5 is being able to "exactly" obtain the object given the function F_R, which is defined after (2.8) in [2]. Equation (5.6) was presented in [2] to provide this step. However, a second method, which is independent of (5.6), was given in [2] for inverting F_R. This method is indicated by the lower half of the right circle in figure 3 in [2]. Hence, statement 5 remains unaffected.

From reading [1], one might conclude that without using (5.6), inverting the function F_R is by necessity "awkward." This is not the case. Rather than using (5.6) one can use the method indicated by the lower loop of the circle on the right in Fig. 3 of [2]. This would involve first using (5.2) to generate all the line integrals perpendicular to the z axis. Then the object would be obtained by performing a two-dimensional Radon inversion on each plane that is perpendicular to the z axis.

From the computational viewpoint, the method indicated by the lower circle on the right in Fig. 3 in [2] has its advantages and disadvantages. An advantage is its computational efficiency. By examining (5.2) in [2] it is observed that the discrete implementation of this method requires four embedded loops: two for the ϕ and θ variables associated with the unit vector β, and two more for the two rectangular variables perpendicular to the vector $\varphi_\perp$. (Please see (5.2) in [2].) In contrast, five embedded loops are needed for (5.6); two for the ϕ and θ variables associated with the unit vector β, and three more for the three-dimensional rectangular reconstruction grid. Although this method has a relative advantage with respect to

Manuscript received August 14, 1992; revised January 28, 1993.

The author is with the Tomographic Imaging Laboratory, University of Cincinnati, Cincinnati, OH 45221-0025.

IEEE Log Number 9210303.